Impact of thermoelectric phenomena on phase-change memory performance metrics and scaling

2012 Nanotechnology 23 205201

(http://iopscience.iop.org/0957-4484/23/20/205201)

Nanotechnology **23** (2012) 205201 (7pp) doi:10.1088/0957-4484/23/20/205201

Impact of thermoelectric phenomena on phase-change memory performance metrics and scaling

Jaeho Lee, Mehdi Asheghi and Kenneth E Goodson

Department of Mechanical Engineering, Stanford University, Stanford, CA 94305, USA

E-mail: zeost@stanford.edu (J Lee)

Received 3 February 2012, in final form 20 March 2012
Published 30 April 2012
Online at stacks.iop.org/Nano/23/205201

Abstract

The coupled transport of heat and electrical current, or thermoelectric phenomena, can strongly influence the temperature distribution and figures of merit for phase-change memory (PCM). This paper simulates PCM devices with careful attention to thermoelectric transport and the resulting impact on programming current during the reset operation. The electrothermal simulations consider Thomson heating within the phase-change material and Peltier heating at the electrode interface. Using representative values for the Thomson and Seebeck coefficients extracted from our past measurements of these properties, we predict a cell temperature increase of 44% and a decrease in the programming current of 16%. Scaling arguments indicate that the impact of thermoelectric phenomena becomes greater with smaller dimensions due to enhanced thermal confinement. This work estimates the scaling of this reduction in programming current as electrode contact areas are reduced down to 10 nm × 10 nm. Precise understanding of thermoelectric phenomena and their impact on device performance is a critical part of PCM design strategies.

(Some figures may appear in colour only in the online journal)

1. Introduction

The temperature fields in semiconductor nanostructures, as well as their performance and reliability metrics, can be strongly influenced by thermoelectric phenomena [1–6]. The impact can be particularly large in phase-change memory (PCM) devices, which experience temperature excursions exceeding 600 °C [7] and current densities up to 10^8 A cm^{-2} with a carbon nanotube electrode demonstrated by Pop *et al* [8]. These extreme electrical and thermal conditions both increase the relevance of thermoelectric transport and provide an ideal opportunity for studying their impact. In a recent paper, we developed the first measurements of the Seebeck and Thomson coefficients of phase-change material films down to 25 nm using a microfabricated silicon-on-insulator device [9]. The present paper uses representative data from this past study to determine the impact of thermoelectric phenomena in PCM devices and quantify their impact on the programming current using electrothermal simulations.

Recent measurements provide evidence for thermoelectric effects in PCM devices. Castro *et al* demonstrated a shift of the amorphous region in lateral PCM cells by switching the bias polarity [1]. The Thomson effect yields heat absorption or release in a medium carrying an electrical current while sustaining a temperature gradient. The position of the amorphous region changes with the bias polarity in PCM cells because Thomson heating alters the temperature distribution during the reset operation. The bias-polarity-dependent behavior was also shown by Suh *et al* in vertical PCM cells while testing different electrode materials [2]. Their cell performance varies for the electrode material with different Seebeck coefficient due to another thermoelectric effect, known as the Peltier effect. The Peltier effect yields heat absorption or release near a material interface which passes an electrical current. PCM cells with electrode and phase-change materials that have a large difference in the Seebeck coefficient can generate strong Peltier heating and reduce the programming current.

	σ [S/m]	k [W/mK]
W	2 X10^7	174
GST-c	10^5	0.7
GST-a	10^2	0.2
TiN	10^6	10
SiO_2	10^{-14}	1.4
Si	10^{-12}	149

Thermal boundary resistance (R_B) of GST is given as 20 x 10^{-9} m^{2}K/W

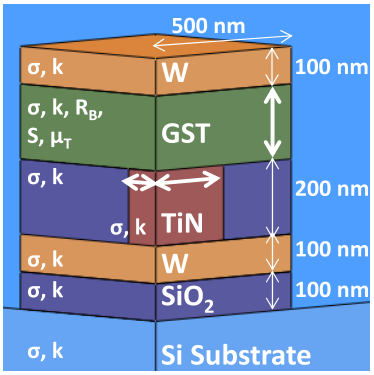

Figure 1. Schematic of the model geometry and material properties used in the simulations. The model represents a quarter-cut cell of a mushroom-type PCM. The Seebeck coefficient (S) and the Thomson coefficient (μ_T) of GST are varied to demonstrate their impact on the reset simulations. The thickness of the GST layer is also varied, from 500 to 50 nm, and the contact area of the TiN electrode is varied from 300 nm × 300 nm to 10 nm × 10 nm to study the impact of device scaling.

Here we simulate PCM devices with careful attention to both Peltier and Thomson heating and the resulting impact on the programming current during the reset operation. Among the many designs of PCM, this paper focuses on a mushroom-type vertical PCM structure (figure 1). Thermoelectric phenomena are not evident in most lateral structures because the Peltier effect is negligible in large electrode contacts and the Thomson effect shows no bias polarity dependence with symmetric geometries. Vertical cells are more relevant for the PCM industry because of the higher density storage and greater susceptibility to thermoelectric heating due to asymmetric geometries. The simulations include geometric variations of electrode contact area from 300 nm × 300 nm to 10 nm × 10 nm and phase-change layer thickness from 500 to 50 nm, and we explain the geometric effects associated with thermoelectric heating through qualitative scaling arguments. This paper provides a comprehensive description of thermoelectric phenomena, including the Thomson and the Peltier effects in PCM devices, and estimates their relative influence on the temperature distribution and programming current during the reset operation.

2. Electrothermal modeling of phase-change memory

2.1. Simulation details

There have been a number of simulations developed for PCM cells, including the one-dimensional (1D) conduction model [10], 2D cylindrical model [11], and 3D cylindrical [12] and Cartesian [13] models, that can handle switching dynamics of phase-change material as well as its electrical and thermal characteristics. Most models calculate the temperature distribution of PCM cells by solving heat diffusion and Joule heating equations. This approach is only valid when the simulation length scales are much larger than the carrier mean free path and when the thermoelectric effects are negligible. Our simulations consider thermoelectric phenomena by solving the following version of the heat conduction equation,

$$C\frac{\partial T}{\partial t} = \nabla(k\nabla T) + q'''_{\text{Joule}} + q'''_{\text{Thomson}} \quad (1)$$

$$q'''_{\text{Joule}} = \rho j^2 \quad (2)$$

$$q'''_{\text{Thomson}} = -\mu_T \nabla T j \quad (3)$$

in which C is the volumetric heat capacity, T is temperature, t is time, k is the thermal conductivity, ρ is the electrical resistivity, j is current density, and μ_T is the Thomson coefficient. The equations (2) and (3) are coupled with the Laplace equation ($\nabla(\sigma\nabla\phi) = 0$, where σ is the electrical conductivity and ϕ is electrical potential). Equation equation (3) captures Thomson heating within a homogeneous material. Our model also simulates Peltier heating by applying the boundary condition

$$q''_{\text{Peltier}} = T\Delta S j \quad (4)$$

at the junction of two materials with the Seebeck coefficient difference ΔS. At the interface, the charge carriers lose energy to the lattice by scattering over a few mean free paths, and the energy distribution can be precisely calculated by Monte Carlo simulations [14]. Peltier heating may spread over a distance due to local Seebeck coefficient variations or non-equilibrium carrier concentrations near the junction [15, 16]. The Peltier effect is simply modeled as a heat source or a heat sink at the junction. This simplification is valid for phase-change materials whose carrier mean free path is much smaller than the cell dimensions and for homogeneous materials with strong carrier recombination [17].

Figure 1 shows a mushroom-type PCM cell that consists of top and bottom W electrode contacts (TEC and BEC, respectively), a phase-change layer (GST), and an electrode plug (TiN) surrounded by electrical passivation (SiO_2). The TEC is biased with a 50 ns electrical pulse while the BEC is grounded; therefore, the current flows through TEC, GST, TiN, and BEC. During the reset operation, a fraction of crystalline GST reaching the melting temperature 600 °C takes the amorphous values. The model assumes the thermal time constant (<10 ns) is short enough to neglect recrystallization upon subsequent quenching. The electrical resistance of the cell is estimated by applying a small voltage across the electrodes and calculating the resulting current density. The programming current is recorded when the cell resistance increases to more than 100 times the original value since the reset-to-set resistance ratio larger than 100 allows reliable array operation of PCM devices [18–20]. This paper does not show simulations for the set operation since the thermoelectric effects have a greater impact on the reset transition of phase-change materials.

2.2. Material properties

The Seebeck coefficient (S) of $Ge_2Sb_2Te_5$ (GST) and related compounds is always positive because the charge carriers

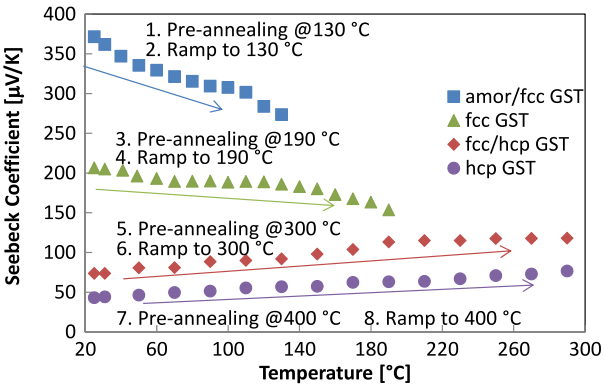

Figure 2. Phase- and temperature-dependent Seebeck coefficient of 125 nm thick GST films as reported previously in [9]. This figure is reproduced here to help explain the selection of material properties for the current simulations. In the amorphous and cubic (fcc) phases, the Seebeck coefficient decreases with increasing temperature, and the Thomson coefficient is negative. In the hexagonal (hcp) phase, the Seebeck coefficient increases with increasing temperature, and the Thomson coefficient is positive.

in p-type semiconductors flow in the same direction as heat. The Thomson coefficient, however, changes sign in the crystalline phase depending on the temperature dependence. The reported Seebeck coefficient of GST alloys varies widely and is measured at room temperature to be as large as 1.5 mV K^{-1} in the amorphous phase [21], 380 μV K^{-1} in the cubic phase [22], and 40 μV K^{-1} in the hexagonal phase [23]. However, there are relatively few data for phase-change materials at the film thicknesses relevant for PCM devices.

Our recent work [9] measured the phase- and temperature-dependent Seebeck coefficient of GST films down to 25 nm thickness. The Seebeck coefficient data (figure 2) show a strong dependence on the phase and temperature. The Seebeck coefficients of amorphous and cubic GST films decrease with increasing temperature by carrier activation and crystallization effects. The Seebeck coefficient of hexagonal GST films increases with increasing temperature due to enhanced scattering with phonons. Because the temperature history and phase quality of crystalline GST films in actual devices are difficult to predict, we take representative values for the Seebeck coefficient and the Thomson coefficient in our simulations. The GST phase in the active region is assumed to be cubic due to the nature of rapid heating in set pulses. The Seebeck coefficient of cubic GST film, pre-annealed at 190 °C, decreases from 206 μV K^{-1} at room temperature to 153 μV K^{-1} at 190 °C. The temperature dependence ($\sim T^{-1}$) extrapolates such that the Seebeck coefficient reduces to $\sim$100 μV K^{-1} near the melting temperature. Simulating PCM devices with a constant Seebeck coefficient 100 μV K^{-1} underestimates Peltier heating and provides a lower bound for the programming current reduction. The Thomson coefficient of fcc GST film is estimated from the Seebeck coefficient data in [9] by the definition $\mu_T = T\partial S/\partial T$ and takes an average value of approximately -100 μV K^{-1}.

Other simulation parameters for the GST film include the thermal boundary resistance (TBR) as well as its electrical and thermal conductivities in each phase (figure 1). Reifenberg *et al* [24] showed that the TBR of GST and TiN can dominate the device thermal resistance and is critical for PCM simulations. Our previous measurements provide detailed information about the thermal and electrical properties of GST as a function of material stoichiometry and grain orientation and size [25–27]. This work uses constant material properties since there are no data available at temperatures above 500 °C. The assumption results in overprediction of the total thermal resistance and underestimation of the programming current.

2.3. Comparison of the simulations to experimental data

To establish confidence in the simulations performed here, we simulated PCM test structures in the literature and compared the simulation results to the experimental data. Suh *et al* [2] had experimentally observed a bias polarity in their PCM cell, which required a programming current 2.3 mA in the forward bias and 3.2 mA in the reverse bias. Simulations for a mushroom-type cell with a 200 nm thick GST layer and a 250 nm diameter TiN electrode (designed after [2]) show a bias polarity by taking into account for the thermoelectric transport. Using the Seebeck coefficient 100 μV K^{-1} in the GST, the simulated cell requires a programming current 2.3 mA in the forward bias and 2.7 mA in the reverse bias. The programming current polarity in the simulation 19% (2.3–2.7 mA) is lower than that in the literature data 39% (2.3–3.2 mA) [2] potentially due to a larger Seebeck coefficient in the real device or other effects contributing to the bias polarity such as electromigration [28].

Suh *et al* [2] attempted to reduce the programming current by changing the electrode material to n-type Si, which has a negative Seebeck coefficient. Our simulation model captures the programming current reduction through enhanced Peltier heating as the Seebeck coefficient difference between GST and electrode materials becomes greater. While their analysis [2] limits attention to the Peltier effect, our simulation model attributes experimental behaviors to both the Peltier and the Thomson effects. The Thomson heating in the 250 nm diameter electrode cell contributes to 5% of the programming current reduction, and we expect greater impact in smaller cell geometries.

Thomson heating can thus play an important role in mushroom-type PCM cells where geometry and temperature distributions are asymmetric. The simulations are consistent with the literature data and provide physical insights into the role of thermoelectric effects. Further analysis of thermoelectric transport in PCM cells is presented in the following sections using our model geometry (figure 1).

3. Thermoelectric effects in PCM

3.1. Impact of thermoelectric properties

Thermoelectric transport can strongly influence the temperature distribution in PCM cells during the reset operation (figure 3). Because the reset temperature governs the formation of the amorphous phase and the resulting cell

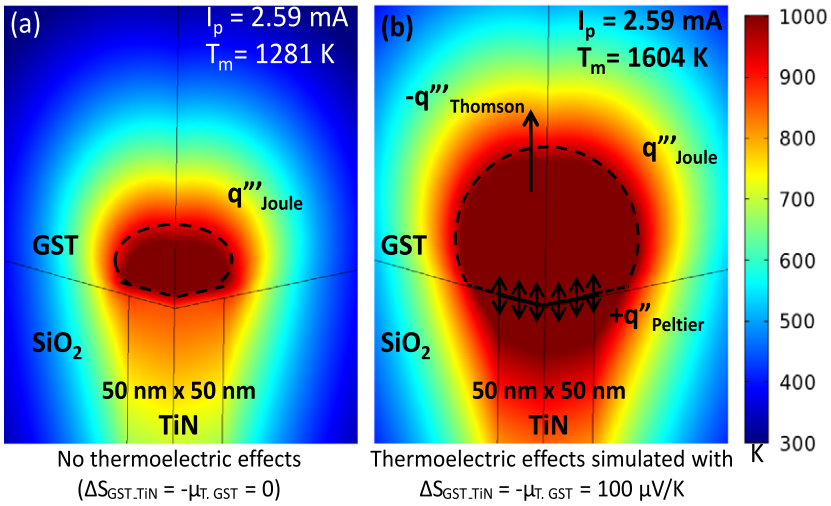

Figure 3. Predicted temperature distributions for 200 nm thick GST device regions with 50 nm × 50 nm TiN electrode structure under the same programming conditions. The dotted region indicates the amorphous phase volume that has temperature exceeding 900 K during the reset operation. Using the Seebeck coefficient 100 μV K^{-1} and the Thomson coefficient -100 μV K^{-1} results in a greater than factor of four larger cell resistance, which requires significantly smaller programming current.

resistance, the thermoelectric heating can effectively lower the programming current required for PCM cells. When current flows from top to bottom through GST and TiN, a positive Seebeck coefficient difference between the GST and the TiN generates Peltier heating that is favorable to reduce the programming current. Figure 4 shows the predicted programming current for a 200 nm thick GST device with a 50 nm × 50 nm TiN electrode structure using the Seebeck coefficient and the Thomson coefficient varying from -200 to 200 μV K^{-1}. The negative Seebeck coefficient is used here, assuming the Seebeck coefficient of electrode material is larger than that of GST. This is consistent with data for heavily doped semiconductors [29, 30]. The programming current decreases linearly with the increasing Seebeck coefficient because Peltier heating is a product of the Seebeck coefficient and the current equation (4).

The programming current has a nonlinear relationship with the Thomson coefficient because Thomson heating depends on the temperature gradient, which also changes with the Thomson coefficient equation (3). When the peak temperature of GST occurs in the vicinity of the TiN interface (figure 3(a)), the temperature gradient is positive in the direction of the current. This condition yields Thomson heating in the GST when the Thomson coefficient is negative. The Thomson heating shifts the peak temperature position away from the TiN interface and expands the amorphous phase volume (figure 3(b)). Figure 4 shows that the negative Thomson coefficient reduces the programming current to some extent. Further increase in the negative Thomson coefficient shifts the peak temperature closer to the TEC, which has a lower thermal resistance, and this requires more current to program the cell. Conversely, a positive Thomson coefficient can be favorable for PCM cells if the peak temperature occurs in the vicinity of the TEC. However, in most mushroom-type PCM cells, the peak temperature occurs near the electrode plug due to the confined geometry and the presence of thermal boundary resistance.

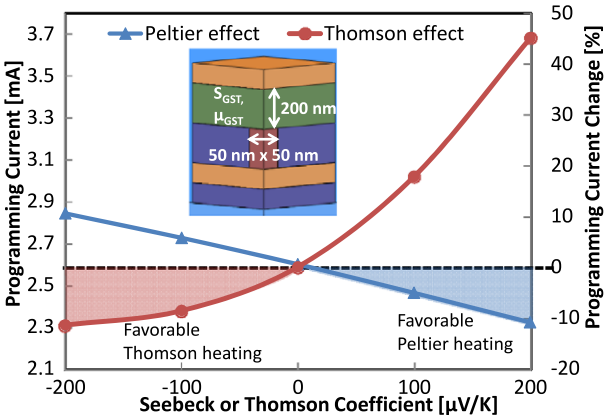

Figure 4. Programming current estimation for the 200 nm thick GST device with 50 nm × 50 nm TiN electrode structure while varying the Seebeck coefficient and the Thomson coefficient from -200 μV K^{-1} to 200 μV K^{-1}, respectively. The negative Thomson coefficient and the positive Seebeck coefficient of GST are favorable for PCM devices assuming the current flows from the top to bottom electrodes. The Seebeck coefficient of the TiN electrode is set to be zero when simulating the Peltier effect.

The Seebeck coefficient and the Thomson coefficient are used as individual parameters here to show the scaling behavior of each thermoelectric effect. However, because the Thomson coefficient is governed by the temperature dependence of the Seebeck coefficient, it is important to keep in mind that these are not truly independent parameters. The programming current reduction by the combined thermoelectric effects reaches up to 15% for the Thomson coefficient -100 μV K^{-1} and the Seebeck coefficient 100 μV K^{-1}. Using phase-change materials with the larger Seebeck coefficient 200 μV K^{-1} and the larger Thomson coefficient -200 μV K^{-1} can reduce the programming current by 26%, which corresponds to a 45% reduction in the power consumption.

3.2. Electrode contact area scaling

PCM technology has demonstrated scalability to smaller dimensions and programming current reduction as a function of electrode contact area [31, 32]. Figure 5 shows the impact of thermoelectric effects during the reset operation with the contact area scaling. The Seebeck coefficient 100 μV K^{-1} and the Thomson coefficient -100 μV K^{-1} are taken from our measurement data (figure 2) assuming the GST is in the cubic phase. The maximum temperature increase (figure 5(a)), compared to a simulation with no thermoelectric effects, represents a ratio of Thomson and Peltier heating to Joule heating. We introduce here a dimensional scaling parameter λ, such that the contact area scales with a factor λ^2 and the current density scales by λ^{-2}. The Joule heating power scales to the square of the current density and by λ^{-4}. Since the second derivative of temperature scales with the Joule heating ($\mathrm{d}^2T/\mathrm{d}x^2 \sim q_{\mathrm{Joule}} \sim \lambda^{-4}$), the temperature gradient scales by λ^{-3} and the temperature scales by λ^{-2}. The Thomson heating ($-\mu_{\mathrm{T}} J \mathrm{d}T/\mathrm{d}x \sim \lambda^{-5}$) and the Peltier heating ($\Delta SJT/\lambda \sim \lambda^{-5}$) both scale faster than the Joule heating. The thermoelectric heating to Joule heating ratio then scales by λ^{-1} with the scaling factor and by $\lambda^{-0.5}$ with the contact area. The temperature changes due to thermoelectric effects increase up to 40% as the contact area scales down to 15 nm $\times$ 15 nm. Further scaling generates significant Joule heating in the electrode instead of the phase-change material. With a shorter or more conductive electrode, the impact of thermoelectric heating can continue to increase with contact area scaling.

The changes in temperature do not lead directly to programming current changes. The programming current reductions require the effective position and shape of the amorphous phase volume. Although the maximum temperature change due to the Peltier effect increases with scaling (figure 5(a)), the programming current reduction due to the Peltier effect does not show appreciable changes (figure 5(b)). This is because the relative amount of GST region heated above the melting temperature does not change substantially with the contact area scaling.

The impact of Thomson effect on programming current varies widely with the contact area because the scaling changes the position of the amorphous phase volume. When the contact area is larger than 50 nm $\times$ 50 nm, the maximum temperature occurs near the middle of GST film, and the Thomson effect can potentially leave a significant amount of the crystalline GST near the electrode interface. For instance, in the 100 nm $\times$ 100 nm contact area cell, Thomson heating achieves a larger temperature rise compared to Peltier heating but produces a smaller cell resistance. When the contact area is smaller than 50 nm $\times$ 50 nm, the maximum temperature occurs near the electrode interface, and Thomson heating continues to reduce the programming current by creating the larger amorphous phase volume.

3.3. GST thickness scaling

The simulation results compare the electrode contact area scaling of the 200 nm thick GST device to that of the 50 nm thick GST device. The GST thickness scaling intensifies Thomson heating by creating a steeper temperature gradient and reduces the programming current. The thermoelectric transport increases the GST peak temperature up to 44% and decreases the programming current up to 16%, which corresponds to a 30% reduction in the power consumption. The impact of GST thickness scaling is more evident when the thermal healing length reaches the TEC interface, i.e., when the contact area is larger than 100 nm $\times$ 100 nm. However, the further thickness scaling may cause a significant temperature drop in the TEC instead of the GST, which can result in weaker Thomson heating.

The GST thickness scaling increases the impact of Peltier heating on device temperature by scaling down the Joule heating volume as long as the interface temperature remains constant. When the peak temperature position shifts away from the interface, i.e., when the contact area is larger than 100 nm $\times$ 100 nm, the GST thickness reduction decreases the interface temperature, which results in weaker Peltier heating. However, figure 5(b) shows no differences in the

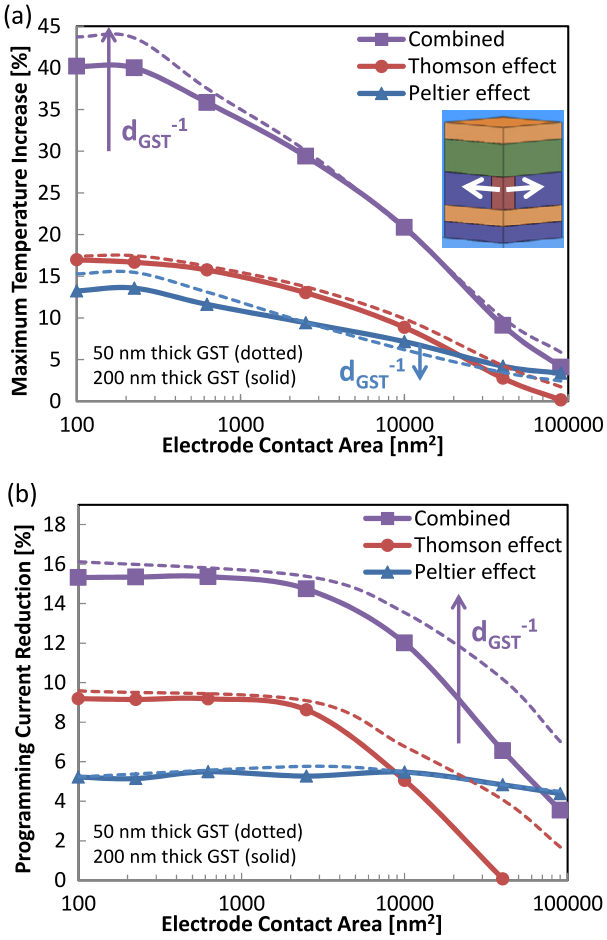

Figure 5. Impact of thermoelectric transport on the maximum temperature (a) and the programming current (b) for the reset operation of PCM cells with TiN electrode contact area scaling from 300 nm $\times$ 300 nm to 10 nm $\times$ 10 nm. The Seebeck coefficient and the Thomson coefficient of GST are set to 100 μV K^{-1} and -100 μV K^{-1}, respectively. The changes in temperature and programming current are calculated with respect to a simulation with no thermoelectric effects.

programming current change by the Peltier effect between the two GST thicknesses because Peltier heating does not change the shape of the amorphous phase. The simulations here assume that the material properties do not scale with the GST thickness, which is consistent with our experimental observation for GST film thickness of 50 nm and above [9].

4. Discussion

Our simulation results show the programming current reductions are made possible by incorporating thermoelectric properties of PCM materials. The thermal boundary resistance (TBR) is another property that has drawn the attention of materials engineering [24]. When the Thomson effect is coupled with a large TBR, the temperature gradient within the GST becomes steeper, and consequently its impact on the programming current becomes greater. The large TBR, however, can reduce the Peltier heating by producing a low interfacial Seebeck coefficient [16].

The TBR and the Peltier effect are both capable of improving the thermal efficiency at the interface, but in different ways. While the TBR increases the total thermal resistance by accounting for the acoustic mismatch, the Peltier effect generates additional heating by compensating for the Seebeck coefficient mismatch. The latter increases the volume of the amorphous phase without changing its shape. Depending on the geometry, improving Peltier heating can be more effective in reducing the programming current than increasing the TBR. For example, simulations for a 200 nm thick GST device with 50 nm × 50 nm TiN electrode structure show that the Seebeck coefficient of 50 μV K^{-1} achieves an equivalent programming current reduction with the TBR of 2×10^{-7} m^2 K W^{-1}, which is a fairly large value for typical PCM materials.

For GST structures, contact electrode materials with negative Seebeck coefficient (e.g. n-type poly-Si or Si–Ge) can maximize the Seebeck coefficient difference and Peltier heating. The reported Seebeck coefficient of nanostructured Si–Ge alloy reaches up to -260 μV K^{-1} at 600 °C [33]. Control of grain structure and carrier energy filtering can further increase the Seebeck coefficient [34]. Our study suggests that carefully engineered electrode and phase-change materials can significantly improve the thermal efficiency of PCM devices through thermoelectric heating. The thermoelectric properties as well as thermal and electrical properties of PCM materials present a rich set of possibilities for optimizing the device performance. Appropriate measurements should reveal the electron–phonon transport physics and identify their contributions in the PCM materials.

The PCM community is on the move at improving the data retention by using phase-change materials (e.g. GeSb [35], GeTe [36], and GaSb [37]) with high crystallization and melting temperatures. Equations (3) and (4) show that the thermoelectric heating favors large temperature. With the increased temperature budget, the impact of Thomson and Peltier effects may become greater. The thermoelectric effects will continue to be important for PCM devices as long scalability and data retention remain their key attributes.

5. Conclusion

This paper qualitatively describes the impact of thermoelectric phenomena in PCM devices and quantitatively predicts the programming current reductions for mushroom-style device geometries. The simulation results show that the programming current can be significantly reduced through Thomson heating within the phase-change material and Peltier heating at the electrode interface. The impact of thermoelectric effects becomes greater with the electrode contact area scaling due to the increased current density and the thermal confinement. Our scaling arguments predict that the thermoelectric effects will continue to be important with device scaling to smaller dimensions.

This paper indicates that precise understanding of the thermoelectric effects in PCM devices is necessary for effective device engineering. Accurate measurements of the Seebeck coefficient and its temperature dependence will improve device simulations and design strategies by delivering a full picture of temperature distributions. Our work demonstrates that there are potentially strong thermoelectric effects in the existing PCM structures, especially those with confined geometries. The simulation results and the analysis discussed here provide physical insights into thermal phenomena and cell optimization opportunities for novel phase-change memory geometries. The controlled thermoelectric heating in the phase-change region can lead to significant reductions in programming power, which can be a breakthrough for PCM technology.

Acknowledgments

The Stanford authors appreciate support from Intel Corporation, the Semiconductor Research Corporation through contract 2009-VJ-1996, and the National Science Foundation through grant CBET-0853350.

References

[1] Castro D T, Goux L, Hurkx G A M, Attenborough K, Delhougne R, Lisoni J, Jedema F J, Zandt M A A t, Wolters R A M and Gravesteijn D J 2007 Evidence of the thermo-electric Thomson effect and influence on the program conditions and cell optimization in phase-change memory cells *IEDM Tech. Dig.* 315–8

[2] Suh D-S, Kim C, Kim K H P, Kang Y-S, Lee T-Y, Khang Y, Park T S, Yoon Y-G, Im J and Ihm J 2010 Thermoelectric heating of $Ge_2Sb_2Te_5$ in phase change memory devices *Appl. Phys. Lett.* **96** 123115

[3] Bakan G, Khan N, Cywar A, Cil K, Akbulut M, Gokirmak A and Silva H 2011 Self-heating of silicon microwires: crystallization and thermoelectric effects *J. Mater. Res.* **26** 1061–71

[4] Grosse K L, Bae M-H, Lian F, Pop E and King W P 2011 Nanoscale joule heating, peltier cooling and current crowding at graphene-metal contacts *Nature Nanotechnol.* **6** 287

[5] Jungen A, Pfenninger M, Tonteling M, Stampfer C and Hierold C 2006 Electrothermal effects at the microscale and their consequences on system design *J. Micromech. Microeng.* **16** 1633–8

[6] Kim D-K and Park Y 2010 Polarity-dependent morphological changes of Ti/TiN/W via under high current density *IEEE Electron Device Lett.* **31** 120–2

[7] Yamada N, Ohno E, Nishiuchi K and Akahira N 1991 Rapid-phase transitions of GeTe-Sb2Te3 pseudobinary amorphous thin films for an optical disk memory *J. Appl. Phys.* **69** 2849–56

[8] Xiong F, Liao A, Estrada D and Pop E 2011 Low-power switching of phase-change materials with carbon nanotube electrodes *Science* **332** 568–70

[9] Lee J, Kodama T, Won Y, Asheghi M and Goodson K E 2012 Phase and temperature dependent thermoelectric properties of $Ge_2Sb_2Te_5$ films down to 25 nm thickness *J. Appl. Phys.* under review

[10] Kang D-H, Ahn D-H, Kim K-B, Webb J F and Yi K-W 2003 One-dimensional heat conduction model for an electrical phase change random access memory device with an $8F^2$ memory cell ($F = 0.15\ \mu$m) *J. Appl. Phys.* **94** 3536–42

[11] Cai D, Song Z, Chen H and Chen X 2011 Temperature model for $Ge_2Sb_2Te_5$ phase change memory in electrical memory device *Solid-State Electron.* **56** 13–7

[12] Li Y, Hwang C H, Li T Y and Cheng H W 2009 Temperature model for $Ge_2Sb_2Te_5$ phase change memory in electrical memory device *Nanotechnology* **20** 285701

[13] Kim D-H, Merget F, Forst M and Kurz H 2007 Three-dimensional simulation model of switching dynamics in phase change random accessmemory cells *J. Appl. Phys.* **101** 064512

[14] Ng W Ch, Liu Y and Hess K 2004 Lattice temperature model and temperature effects in oxide-confined VCSELs *J. Comput. Electron.* **3** 103–16

[15] Price P J 1956 Theory of transyort effects in semiconductors thermoelectricity *Phys. Rev.* **104** 1223

[16] da Silva L W and Kaviany M 2004 Microthermoelectric cooler: interfacial effects on thermal and electrical transport *Int. J. Heat Mass Transfer* **47** 2417–35

[17] Lashkevych I, Cortes C and Gurevich Yu G 2009 Physics of thermoelectric cooling: alternative approach *J. Appl. Phys.* **105** 053706

[18] Kim S, Zhang Y, McVittie J P, Jagannathan H, Nishi Y and Wong H-S P 2008 Integrating phase-change memory cell with Ge nanowire didoe for crosspoint memory—experimental demonstration and analysis *IEEE Trans. Electron Devices* **55** 2307–13

[19] Liu B, Song Z T, Feng S L and Chen B M 2005 Characteristics of chalcogenide nonvolatile memory nano-cell-element based on Sb2Te3 material *Microelectron. Eng.* **82** 168–74

[20] Qiao B, Feng J, Lai Y, Cai Y, Lin Y, Tang T, Cai B and Chen B 2007 Phase-change memory device using Si–Sb–Te film for low power operation and multibit storage *J. Electron. Mater.* **36** 88

[21] Baily S A, Emin D and Li H 2006 Hall mobility of amorphous $Ge_2Sb_2Te_5$ *Solid State Commun.* **139** 161

[22] Kato T and Tanaka K 2005 Electronic properties of amorphous and crystalline $Ge_2Sb_2Te_5$ films *Japan. J. Appl. Phys.* **44** 7340–4

[23] Yan F, Zhu T J, Zhao X B and Dong S R 2007 Microstructures and thermoelectric properties of GeSbTe based layered compounds *Appl. Phys.* A **88** 425

[24] Reifenberg J P, Kencke D L and Goodson K E 2008 The impact of thermal boundary resistance in phase-change memory devices *IEEE Electron. Device Lett.* **29** 1112–4

[25] Reifenberg J P, Chang K-W, Panzer M A, Kim S, Rowlette J A, Asheghi M, Wong H-S P and Goodson K E 2010 Thermal boundary resistance measurements for phase-change memory devices *IEEE Electron Device Lett.* **31** 56–8

[26] Lee J, Li Z, Reifenberg J P, Asheghi M and Goodson K E 2011 Thermal conductivity anisotropy and grain structure of $Ge_2Sb_2Te_5$ films *J. Appl. Phys.* **109** 084902

[27] Lee J, Kim S, Jeyasingh R, Asheghi M, Wong H-S P and Goodson K E 2011 Microthermal stage for electrothermal characterization of phase-change memory *IEEE Electron. Device Lett.* **32** 952–4

[28] Kim C, Kang D M, Lee T Y, Kim K H P, Kang Y S, Lee J, Nam S W, Kim K B and Khang Y 2009 Direct evidence of phase separation in $Ge_2Sb_2Te_5$ in phase change memory devices *Appl. Phys. Lett.* **94** 193504

[29] Kodato S 1985 Si–Ge alloy film with very high electrical conductivity and thermoelectric power *J. Non-Cryst. Solids* **77/78** 893–6

[30] Yamashita O 2004 Effect of metal electrode on seebeck coefficient of p- and n-type silicon thermoelectrics *J. Appl. Phys.* **95** 178–83

[31] Raoux S *et al* 2008 Phase-change random access memory: a scalable technology *IBM J. Res. Dev.* **52** 465–79

[32] Wong H-S P, Raoux S, Kim S, Liang J, Reifenberg J P, Rajendran B, Asheghi M and Goodson K E 2010 Phase change memory *Proc. IEEE* **98** 2201

[33] Wang X W *et al* 2008 Enhanced thermoelectric figure of merit in nanostructured n-type silicon germanium bulk alloy *Appl. Phys. Lett.* **93** 193121

[34] Medlin D L and Snyder G J 2009 Interfaces in bulk thermoelectric materials *Curr. Opin. Colloid Interface Sci.* **14** 226–35

[35] Raoux S, Cabral J C, Krusin-Elbaum L, Jordan-Sweet J L, Virwani K, Hitzbleck M, Salinga M, Madan A and Pinto T L 2009 Phase transitions in Ge–Sb phase change materials *J. Appl. Phys.* **105** 064918

[36] Perniola L *et al* 2010 Electrical behaviour of phase change memory cells based on GeTe *IEEE Electron Device Lett.* **31** 488–90

[37] Lu Y, Song S, Song Z and Liu B 2011 $Ga_{14}Sb_{86}$ film for ultralong data retention phase-change memory *J. Appl. Phys.* **109** 064503